Water resistant soil stabilization via a mussel mimicry ultra-low swelling hydrogel

Zhi Zhao (zhaozhi@bjut.edu.cn)
Beijing University of Technology https://orcid.org/0000-0002-4491-7641

Yupeng Shan
Beijing University of Technology

Haibin Wang
Beijing University of Technology

Hao Lu
Beijing University of Technology

Xuemei Liu
Beijing University of Technology

Bowen Wang
Beijing University of Technology

Xiaoyan Song
Beijing University of Technology https://orcid.org/0000-0003-3844-729X

Article

Keywords: Soil stabilization, hydrogel stabilizer, mussel mimicry, ultra-low swelling, water resistant

Posted Date: April 26th, 2022

DOI: https://doi.org/10.21203/rs.3.rs-1561398/v1

Abstract

Employing hydrogels as a substitute for cement in soil stabilization is believed to have great environmental benefits. However, current hydrogel soils stabilizers cannot function properly in wet conditions due to swelling induced structural deformation and mechanical weakening, which significantly limits their applications. Inspired by the mussel byssal, we developed a water resistant hydrogel soil stabilizer that worked under all environments. The synergic effect of intermolecular hydrogen bonding and hydrophobic interactions led to the formation of heterogeneous mussel mimicry microstructures that possessed superior toughness and ultra-low swelling ratio. Soils strengthened with such hydrogels maintained great strength in water, which had never been achieved before. The intrinsic water affinity of hydrogels also ensured a decent permeability and retention ability of water, which was critical to ecosystems. The present work holds great promise for developing the next generation environment-insensitive and ecofriendly soil stabilizers.

1. Introduction

Geologic hazards and environmental degradation that arise from soil instabilities have become an increasingly wide spreading global issue. Foundation settlement and landslide, for example, are commonly originated from the loss of strength and stiffness in water-saturated soils, which could cause thousands of death per year over the world.[1] Meanwhile, overly-dried soils may lead to other problems. Cohesionless dry soil particles are the main source of wind-borne fugitive dust, which are known to have extensive negative impacts on human health and safety, including environmental contamination, respiratory ailments and traffic hazards.[2] As a result, efficient soil stabilization solutions that can simultaneously work under all types of climates are highly desirable.

Traditional soil stabilization mainly relies on cement and concrete materials, whose production and application involve heavy machinery and intensive energy consumption.[3] This in turn leads to elevated CO_2 and waste emissions, making the method itself another environmental issue. Recently, great efforts have been spent on the development of cement substitutes to stabilize soil in a more environmentally friendly way.[4] In particular, using hydrogel as a soil binder has shown great advantages. Hydrogels are natural or synthetic polymer networks with extraordinary water affinity, which are able to retain water that is tens to thousands of times of its own weight.[5] Previous researches showed that hydrogel stabilized soils could achieve superior strengths of up to 5.5 MPa, which was comparable to conventional Portland cement.[6] The application of hydrogel stabilizer was also easy and fast. Typically, a hydrogel precursor could be prepared and poured directly into the soil, which then in-site solidified in hours to strength areas of interest. Moreover, many raw materials of hydrogels are readily to obtain. For instance, guar, xanthan and other biopolymers can be extracted from plants,[7] which dramatically reduced the demands on nonrenewable resources.

Despites of these merits, all current hydrogel stabilizers are extremely sensitive to water.[7] Due to their hydrophilic nature, hydrogel materials tend to swell intensively in water, which in turn leads to significant structural deformation and greatly weakened mechanical properties.[7] As a result, previously reported hydrogel stabilizers could only properly function in dry climates.[11–13] Their applications under wet or humid conditions remain a technical bottleneck.

Living creates have evolved efficient strategies to strength soils under all conditions. Mussels, for example, employ byssal threads to anchor themselves on the ground. The byssal thread features heterogeneous micro-structures composed of various tightly associated proteins, which not only provide balanced hardness, elasticity and adhesivity but also allow for great water-resistivity.[7] Consequently, mussels are able to efficiently stabilize sand particles and stay on loose surfaces under repeated tides, making them adaptive to the environment at the shore regions.

Inspired by nature, we developed a novel water resistant hydrogel soil stabilizer that possessed a mussel mimicry heterogeneous microstructure. Morphological and molecular studies have been conducted to reveal the formation mechanism of this unique pattern. The mussel mimicry hydrogel featured ultra-low swelling ratio and superior toughness, all comparable to that of the native mussel byssal. Mechanical tests revealed that sand columns stabilized by such hydrogels maintained great mechanical strength in water, which had never been achieved in previous studies. Beyond that, the environmental stability and water retention ability of hydrogel stabilized soils were analyzed to verify their compatibility with ecosystems. The results indicate that the present work holds great promise for the development of a robust, environment-insensitive and ecofriendly soil stabilizer.

2. Methods

2.1 Materials

Methacrylic acid (MAAc, 99%), acrylic acid (AAc, 99%), acrylamide (AAm, 99%) and dimethylsulfoxide (DMSO, ≥ 99.5%) were purchased from Shanghai Macklin Biochemical Co., Ltd. N,N'-methylenebisacrylamide (Bis, 99%), ammonium persulfate (APS, 99.99%), tetramethylethylenediamine (TEMED, 99%) and fluorescein O-methacrylate (97%) were purchased from Beijing MREDA Technology Co., Ltd.. China ISO standard sand (96+% silica, 0.5-2 mm) was purchased from Xiamen ISO standard sand Co., Ltd.

2.2 Sample preparation

The ultra-low swelling hydrogels were made out of MAAc and AAm, i.e. p(MAAc-co-AAm). First, stock solutions of MAAc and AAm were prepared, whose concentrations were 48.9 wt% and 44.4 wt%, respectively. Next, the two stock solutions were mixed at a certain ratio together with Bis and TEMED. To that mixture, 10 wt% APS was added to trigger the curing process. The precursor was left undisturbed for a day to allow complete gelation. The actual recipe of precursors was tuned according to different experimental purposes. A list of all recipes was included in the supplementary information (Table S1). To

improve the visibility of hydrogel under microscope, fluorescein O-methacrylate might be added into the precursor to fluorescently label samples. To do this, 50 mg fluorescein O-methacrylate was first dissolved in 1 mL DMSO to make a stock solution. The stock solution was then mixed with gel precursors at a 1:100 volume ratio. For tensile tests, the gel precursor was cast within a mold to get bone-shaped samples. For comparison purpose, hydrogels composed of AAc and AAm were also prepared, i.e. p(AAc-co-AAm). Those hydrogels were prepared by replacing the MAAc stock solution by a 44.8 wt% AAc solution while keeping the other factors in the recipe the same.

For soil stabilization trials, ISO standard sand was employed as a model system. The sand was first packed into a column in a tubular container. Hydrogel precursors were immediately poured into the sand once the APS solution was added. The precursor to sand ratio was fixed at 15 mL per 75 g sand. After that, the container was knocked generally for a couple of minutes to remove gas bubbles. Depending on the composition, the precursor cured within 2–24 hours. Once the gel was fully cured, the sand column was taken out of the container and dried in air for 5 days prior to other tests.

The water resistance of pure hydrogels and hydrogel stabilized sand columns was investigated by soaking freshly prepared samples in DI water. The mechanical properties of soaked samples were tested every few hours. For comparison purpose, sand columns stabilized with pure pAAM hydrogel were also made. The recipe of pAAm precursors was listed in Table S1.

2.3 Characterization methods

Microscopic characterizations were carried out on a Leica DM6 microscope. Pure hydrogel was molded into a ~ 100 μm thin layer and checked under the microscope. Hydrogel stabilized sands columns were crushed into millimeter sized granules before characterization. Infrared (IR) spectra of samples were recorded by a FT-IR spectrometer in the total internal reflection mode (PerkinElmer B420). All samples were sliced into thin layers and completed dried prior to spectral measurements. SEM characterizations were performed with a Nova NanoSEM 200 system. The elemental composition of a given area was determined by energy dispersive x-ray spectroscopy (EDX). Prior to SEM analysis, all the sample was coated with a ~ 10 nm layer of gold by a metal evaporator (Bühler Leybold Optics) to improve the electrical conductivity. Tensile tests were performed with an Instron 5948 Micro Tester at a speed of 10 mm/min. Unconfined compressive strength (UCS) of samples was obtained using a uniaxial testing machine (Nanfangjinke, NKK-4050). The compression speed was set at 2 mm/min. Micro-scale hardness measurement was performed by an atomic force microscope (Bruker Multimode 8). Representative regions to be studied were first located under contact mode. The force curve at the regions of interest was then obtained and processed through the NanoScope Analysis 1.8 software to get quantitative data.

2.4 Environmental compatibility tests

The thermostability of hydrogel fixed sand columns was examined by placing samples in a vacuum oven (Shenzhen Kejing Star Technology, DZF-6020). The samples were heated at 60°C for 7 days and their mechanical strength was investigated by UCS measurements. Some columns were then soaked in water and heated in oven again. The mechanical strength change during the soaking-heating cycles was also

characterized. UV stability test was conducted by placing the column under a UV light source (FUWO FXLite 320). The mechanical strength at various exposure times was recorded. Pure hydrogel was also treated with the UV light. Its IR spectrum was recorded to check for photodegradation. A mini-disk infiltrometer (Decagon) was employed to conduct the water infiltration test. The infiltrometer was filled up with water and directly placed onto large soil columns whose diameter and height was about 10 cm and 5 cm, respectively. The water level inside the infiltrometer was recorded every 10 s until the whole column was saturated. Water retention ability of stabilized soil columns was characterized by measuring the weight change of a fully swollen column with time. The weight change of water saturated sand was also recorded as a control.

3. Results And Discussions

3.1 In-situ formation of mussel mimicry hydrogel structures

Mussels are well known for their ability to stick to loose surfaces under all environmental circumstances. It has been proved that the unique microstructure of mussel byssal plays the critical role.[19,20] A single byssal thread consists a core, a cuticle and a plaque, each of which has distinctive features (Fig. 1a). The cuticle possesses granular appearance and a high hardness to serve as a protective layer. The core has densely packed array of collagenous fibers that help with energy damping. The porous plaque provides strong under-water adhesion to anchor mussels on beach and rocks.

By pouring a carefully engineered hydrogel precursor (e.g. E7 or H1) into sands, we discovered that a mussel mimicry structure could form via in-situ polymerization (Fig. 1b). The spatial distribution as well as the morphology of the hydrogel was characterized by SEM (Fig. S1). The hydrogel dispersed between soil particles exhibited a core-shell feature. The outmost layer of the hydrogel was composed of micro- and submicron-sized granule while the inner part appeared to be bundled fibers, which resembled the byssal cuticle and core. Highly porous patterns were discovered at the hydrogel-soil interfaces, which was similar as the byssal plaque. This mussel mimicry structure was believed to form under the synergic effect of hydrogen bonding and hydrophobic interactions (Fig. 1c). Due to the presence of carboxyl acid and primary amide groups on the polymer chain, intermolecular hydrogen bonding would form.' Meanwhile, the presence of methyl group on MAAc could induce hydrophobic assemblies. The combination of these two non-covalent interactions could re-shape the polymer chains and cause polymer aggregations, phase separations, etc., leading to the unique hydrogel structure found in this research.

3.2 Characteristic properties of the mussel mimicry hydrogel

The swelling of the mussel mimicry hydrogel might be restricted to a very low level though the combination of multiple effects. Hydrogen bonding enhanced the interaction between hydrophilic groups,

thus reduced the absorption of water. The existence of hydrogen bonds in the p(MAAc-co-AAm) hydrogel could be readily proved by swelling tests (Fig. 2a). When the total molar concentration of MAAc and AAm was fixed, varying the MAAc to AAm ratio led to significant changes in the swelling ratio. Here the swelling ratio (S_w) was defined by the following equation:

$$S_w = \frac{M_w}{M_i} \times 100\%$$

where M_w and M_i was the swollen weight and initial weight of a hydrogel, respectively. Accordingly, S_w=100% indicated the mass of gel didn't change after soaking (zero swelling). It was observed that the S_w first dropped with increasing MAAc concentrations, reaching a minimal when [MAAc] equaled to [AAm], then increased at high MAAc contents. This clearly evidenced that a great amount of hydrogen bonds formed at proper MAAc to AAm ratios, which served as additional crosslinkers to reduce swelling. FR-IR spectrum indicated that the C = O stretching of carboxyl in the p(MAAc-co-AAm) hydrogel didn't behave as the simple addition of pMAAc and pAAm spectra (Fig. S2), i.e. the simulated spectrum. Instead, it showed a red shift relative to the simulated curve, indicating the bonding between carboxylic acid and amide groups (Fig. 2b).

The methyl group on MAAc was critical to the achievement of ultra-low swelling ratio. First, its hydrophobic nature and spatial vicinity to the carboxyl group could partially block the attack on hydrogen bonds from water molecules, thus prevented the hydration of hydrophilic moieties (Fig. 1c). As a proof, it is discovered that p(MAAc-co-AAm) gel swelled much less than the p(AAc-co-AAm) gel (Fig. 2a). In addition, introducing the methyl group also facilitated the generation of phase separation in the hydrogel. Neighboring methyl groups tended to agglomerate via hydrophobic interactions in order to reduce the exposed area in aqueous media. The blue shift of C-H stretching peaks in the FT-IR spectrum suggested the interactions between methyl groups (Fig. 2b). This would re-organize the polymer chains and lead to the formation of hydrophobic phases. Microscopic image revealed that the p(MAAc-co-AAm) hydrogel had an uneven texture. A vast number of tiny particles could be identified under the dark field mode (Fig. 2c), which corresponded to the granule observed in the SEM (Fig. 2d). The formation of the heterogeneous texture caused strong light scattering, rendering a white, opaque appearance for the hydrogel (Fig. 2c, Inset). The presence of hydrophobic phases further lowered down the swelling ratio of hydrogel. First, gel expansion had to spend additional energy when breaking hydrophobic phases. Moreover, the hydrogen bonds packed much denser in the hydrophobic phase, leaving little space for water molecules to insert in.

The swelling ratio of the hydrogel might be further tuned through adjusting the amount of crosslinkers. With the increase of Bis concentration in the receipt (A series-G series), the S_w value dropped dramatically. Typical S_w of the as-obtained hydrogel ranged from 102%-115%, with zero swelling achieved at 38.5 mg/mL Bis (Fig. S3a). Although the water resistance of hydrogel might benefit from elevated Bis concentrations, keep adding crosslinker would cause some troubles. Chemical crosslinkers such as Bis bridges polymer chains through strong yet brittle covalent bonds. Therefore, the hydrogel would become

less elastic and loose toughness at high Bis concentrations. Compressive tests showed that the UCS of sand columns fixed by high-Bis hydrogels were much weaker in strength (Fig. S3b). The optimum recipe was found at where Bis concentration equaled to 15.4 mg/mL. Interestingly, the gel precursor would cure even without adding Bis (Fig. S3c), which was attributed to the strong intermolecular interactions mentioned earlier (Fig. 1c). In this case the S_w of hydrogel would be tremendous (Fig. S3a).

The impressively low S_w enabled a water stable toughness of the hydrogel. Tensile measurements revealed that the ultimate strength of swollen hydrogel (E7) was almost identical to that of freshly prepared hydrogel (Fig. 2e). Moreover, the strain and toughness of both samples were very close (freshly prepared gel: 210%, 2.1 MJ/m^3; swollen gel: 180%, 1.7 MJ/m^3). This great ability to maintain mechanical strength under water was rarely seen in conventional hydrogels, which constantly suffered from losing toughness upon swelling.' The measured harness and elasticity was also impressive compared with regular tough hydrogels,' which was expected to benefit from the mussel mimicry microstructure. The core-shell structure of as-prepared hydrogels resembled the cuticle and core of mussel byssal (Fig. 2f). AFM tests (Fig. S4) revealed that the granular shell of the hydrogel possessed an extraordinary Young's modulus (E) of 0.60 ± 0.09 GPa, comparative to that of the hard, robust cuticle (~ 2.0 GPa).[20] Similarly, this granular shell of the hydrogel was thought to provide protection for the interior materials. The inner part of the hydrogel exhibited a fibrous texture that was very similar to the core of byssal. Previous researches showed that the byssal core was the main contributor to the elasticity.[19] Being rich in noncovalent interactions, the fibrous interior should also exhibited great flexibility. AFM measurements confirmed that its elastic modulus was 0.15 ± 0.02 GPa, demonstrating the ease of deformation. This value was also on the same level as the byssal core (E = 0.3–0.4 GPa).[20] The combination of the hard shell and the elastic core finally led to great mechanical properties, as proven in both nature (mussel) and synthetic systems (this work).

3.3 The principle of structural evolution in the hydrogel

The formation of the mussel mimicry structure relied on balanced hydrogen bonding and hydrophobic interactions, which required a proper formulation. Varying the MAAc to AAm ratio would lead to completely different results. The interior structure of the hydrogel was predominantly determined by the intermolecular interactions between polymer chains. As shown in Fig. 3a, excessive carboxylic acids or amides might greatly affect the phase separation process. The amide-amide pair is known to have stronger interactions than carboxylic acid pairs due to the existence of a greater number of hydrogen bonding sites, which can be confirmed by the boiling points data. Consequently, excessive amides in the hydrogel tended to pair with themselves, which would facilitate phase separation by excluding water molecules and form densely packed polymer chains. In contrast, excessive carboxyl acids could be better hydrated and helped polymer chains to disperse more uniformly. It is observed that carboxyl acid rich p(MAAc-co-AAm) exhibited a more continuous texture that resembled native byssal thread. The core of the hydrogel consisted of tightly bundled fibrous units, which were likely to be held together by hydrogen bonds between fibers (Fig. 2f & 3b). The surficial layer had a granular appearance. This was expected to

be caused by air exposure induced phase separation. As air is more hydrophobic than aqueous media, it is more energetically favorable for the hydrogel to expose its hydrophobic moiety to the outside. Consequently, tiny hydrophobic domains were formed on the shell (Fig. 2c-2d). In contrast, amide rich hydrogels possessed a more porous feature composed of poorly bundled fibers, demonstrating the preference of self-aggregation within each fibrous unit (Fig. 3c). The porous structure transited to thread-like patterns at the surface due to further collapse of polymer chains in air (Fig. 3d). Due to the reduced interaction between fibrous domains, the amide rich hydrogel had a weaker toughness compared with carboxylic acid rich samples (Fig. 3e), indicating that the mussel mimicry structure was more ideal for mechanical toughness.

Pure hydrogel didn't exhibited the porous structure seen at the vicinity of sand particles. Interestingly, such patterns were dominant when the hydrogel was cured inside the sands. Fluorescent microscopic images showed that the gel layer directly attached to sand surfaces appeared to be highly porous (Fig. 3f), which was consistent with the results in SEM characterizations (Fig. 1b). It was also evident that the porous gel structure had good affinity to the sand since the fracture of sand clusters didn't remove it from the surface. We believed that this phenomenon could be attributed to the hydrophilic nature of the sand particles. It is well known that sand particles usually carried surface charges and are hydrophilic, which may attract ions and water molecules. As a result, the formation of hydrophobic interactions was energetically unfavorable at the surface of sand particles. To adapt to this, the association between methyl groups tended to keep a certain distance away from the surface, leading to the formation of hydrophilic network patterns typically seen in covalently crosslinked hydrogels.[7] It is found from SEM image that the hydrogel structure transited from honeycomb-like patterns to fibrous layers in about 50 microns from sand surfaces (Fig. 3g). The porous feature of the hydrogel at the soil-hydrogel interfaces could be directly visualized at where sand particles got peeled off from the hydrogel stabilizer. The interaction between the sand surfaces and hydrophilic moieties on the polymer backbones helped to tightly anchor the sand particles on hydrogel, and in turn significantly improved its mechanical strength. The above structure and soil stabilization strategy were a close imitation of mussel plaque.

3.4 Soil stabilization with the mussel mimicry hydrogel

Soils stabilized with the mussel mimicry hydrogel showed dramatically improved mechanical properties. Dry sand columns had an ultimate strength of up to 2.9 ± 0.3 MPa (H1), which was reached at a strain level of 6% (Fig. 4a). This was comparative to some of the best reported records.[11,12] Notably, the above samples exhibited an extraordinary under water robustness that had never been reported before. The measured strength and strain at peak strength remained at 0.8 MPa and 8.5% after a 72-hour water immersion (Fig. 4a), which was critical for soil structures to survive under great rainfall or flood. The water saturated sand columns also showed improved elasticity. A considerable level of strength was found even at 18% stain, demonstrating the mussel mimicry hydrogel stabilized soils were hard to break in natural environment. The volume of the columns didn't have measurable variations within experimental error (Fig. 4b). This superior water resistance was attribute to the combination of the ultra-

low swelling ratio and the robust mussel mimicry structure. In comparison, soils stabilized by conventional hydrogels didn't show good water resistance. Sand columns treated by pAAm hydrogel (H4) might reach a high strength at dry state (2.8 ± 0.3 MPa), but lost more than 96% of the strength upon water treatment (Fig. 4c). The obvious volumetric expansion upon water saturation could be directly visualized by eyes (Fig. 4d), which might be detrimental to load-bearing sand units (e.g. foundations, roads, etc.).

3.5 Environmental compatibility of the mussel mimicry hydrogel

Soil samples strengthened by the mussel mimicry hydrogel are highly stable under various environmental conditions, including high temperature, UV irradiation and repeated hydration. Thermostability tests were conducted to investigate how well the gel could survive under elevated temperatures. As can be seen, the mechanical strength of stabilized sand columns didn't show any decrease upon continuous heating at 60°C (Fig. 5a). Even after several soaking-heating cycles, the measured strength still remained at a constant level. UV resistance of the hydrogel and stabilized sand columns was also tested. The intensity of the UV light was set at 200 mW/cm^2, which was about 1000 times greater than that of sunlight. Consequently, a one-hour UV exposure corresponded to 42 days in the real environment. The strength of the sand column didn't show obvious changes after UV exposure up to 4 hours (Fig. 5b). IR characterizations also indicated that the hydrogel was pretty stable under UV irradiation (Fig. 5c). No photodegradation had been found within the test period (4 h) and the spectrum of pristine and UV irradiated hydrogel looked same. A quick test showed that a sand column left outside for a month could easily support a male weighting 70 kg, no matter in the dry or swollen state (Fig. 5d). This indicated that our strategy was suitable for developing environment insensitive soil stabilizers.

A great advantage of hydrogel binders over cements laid in their capability of absorbing and retaining water, which is critical to the growth of plants. Water infiltration tests were conducted to study the water permeability of soils fixed by the mussel mimicry hydrogel (Fig. 5e). At the initial stage, the water entered into the soil at a nearly constant speed, which was defined as the water infiltration rate. As can be seen, the water infiltration rate for hydrogel stabilized sands could reach up to 16 mm/min, demonstrating the porous nature of the entire column. This confirmed that the hydrogel only took up a small portion of the space among sand particles and the voids left could be used to support water collection and living activities. Meanwhile, the water retention ability was also characterized. Due to the intrinsic hydrophilicity of hydrogel, the additional of hydrogel stabilizer could drastically slow down the evaporation of water, as compared to pure sand (Fig. 5f). About 40–50% of water still remained in hydrogel containing columns after sitting in the air for 7 days, which was critical to planting in relatively dry areas. The water loss rate of pure sand almost doubled that of hydrogel stabilized sand, leading to only ~ 20% water left after a week.

4. Conclusions

In summary, we demonstrated the in-situ synthesis of a novel hydrogel binder for water resistant soil stabilization. Ultra-low swelling ratios could be achieved through the synergetic effect of intermolecular hydrogen bonding and hydrophobic interaction induced phase separation. By properly tuning the experimental parameters, a mussel mimicry structure could be obtained. The great strength and toughness of this unique structure was comparable to that of mussel byssal, which could significantly enhance the stability of soils. The merits above led to the first hydrogel based soil stabilizer that could function under all environmental circumstances. Various tests verified that stabilized soil samples maintained superior mechanical properties under dry, wet, hot and UV-intensive conditions. Moreover, the hydrogel stabilizer had the ability to absorb and retain water, which was critical for planting. The present work provides a promising strategy for developing high performance, cement-free soil stabilizers. The successful application of this technique may greatly benefit the environment and ecosystems.

Declarations

Declaration of competing interest

The authors declare that they have no known competing financial interests or personal relationships that could have appeared to influence the work reported in this paper.

Acknowledgements

This work was supported by the National Natural Science Foundation of China (Grant No. 52101032, 51631002 and 51425101). We would like to thank Prof. Hui Yao for providing some of the raw materials.

Supporting material

Additional data necessary to support the conclusions of this paper is available in the supplementary materials, including detailed experimental procedures and characterizations.

References

1. Huang, Y. & Wen, Z. Recent developments of soil improvement methods for seismic liquefaction mitigation. Natural Hazards 76, 1927-1938 (2015).
2. Bogaard, T. A. & Greco, R. Landslide hydrology: from hydrology to pore pressure. Wiley Interdisciplinary Reviews: Water 3, 439-459 (2016).

3. Gelencsér, A. et al. The red mud accident in Ajka (Hungary): characterization and potential health effects of fugitive dust. Environmental Science & Technology 45, 1608-1615 (2011).

4. Parvej, S. et al. Fugitive Dust Suppression in Unpaved Roads: State of the Art Research Review. Sustainability 13, 2399 (2021).

5. Afrin, H. A review on different types soil stabilization techniques. International Journal of Transportation Engineering and Technology 3, 19-24 (2017).

6. Chen, C., Habert, G., Bouzidi, Y. & Jullien, A. Environmental impact of cement production: detail of the different processes and cement plant variability evaluation. Journal of Cleaner Production 18, 478-485 (2010).

7. Roy, A. Soil stabilization using rice husk ash and cement. International Journal of Civil Engineering Research 5, 49-54 (2014).

8. Ghadir, P. & Ranjbar, N. Clayey soil stabilization using geopolymer and Portland cement. Construction and Building Materials 188, 361-371 (2018).

9. Ahmed, E. M. Hydrogel: Preparation, characterization, and applications: A review. Journal of Advanced Research 6, 105-121 (2015).

10. Guo, Y. et al. Hydrogels and hydrogel-derived materials for energy and water sustainability. Chemical Reviews 120, 7642-7707 (2020).

11. Zhao, Z. et al. Biomimetic hydrogel composites for soil stabilization and contaminant mitigation. Environmental Science & Technology 50, 12401-12410 (2016)

12. Lo, C. Y. et al. Durable and ductile double-network material for dust control. Geoderma 361, 114090 (2020).

13. Hamdan, N., Zhao, Z., Mujica, M., Kavazanjian, E. & He, X. Hydrogel-assisted enzyme-induced carbonate mineral precipitation. Journal of Materials in Civil Engineering 28, 0401689 (2016).

14. Rizwan, M., Gilani, S. R., Durani, A. I. & Naseem, S. Materials diversity of hydrogel: Synthesis, polymerization process and soil conditioning properties in agricultural field. Journal of Advanced Research 33, 15-40 (2021).

15. Wen, K. et al. Mechanical behaviors of hydrogel-impregnated sand. Construction and Building Materials 207, 174-180 (2019).

16. Buenger, D., Topuz, F. & Groll, J. Hydrogels in sensing applications. Progress in Polymer Science 37, 1678-1719 (2012).

17. Subramani, R. et al. The influence of swelling on elastic properties of polyacrylamide hydrogels. Frontiers in Materials 7, 212 (2020).

18. Sun, X., Miao, L., Wang, H., Chen, R. & Wu, L. Bio-cementation for the mitigation of surface erosion in loess slopes based on simulation experiment. Journal of Soils and Sediments (2022).

19. Priemel, T., Degtyar, E., Dean, M. N. & Harrington, M. J. Rapid self-assembly of complex biomolecular architectures during mussel byssus biofabrication. Nature Communications 8, 1-12 (2017).

20. Holten-Andersen, N., Fantner, G. E., Hohlbauch, S., Waite, J. H. & Zok, F. W. Protective coatings on extensible biofibres. Nature Materials 6, 669-672 (2007).

21. Zhao, C., Ma, Z. & Zhu, X. X. Rational design of thermoresponsive polymers in aqueous solutions: A thermodynamics map. Progress in Polymer Science 90, 269-291 (2019).

22. Xu, Y. et al. Development of visible-light responsive and mechanically enhanced “smart” UCST interpenetrating network hydrogels. Soft Matter 14, 151-160 (2018).

23. Leung, C. S., Leung, S. S., Tirado-Rives, J. & Jorgensen, W. L. Methyl effects on protein-ligand binding. Journal of Medicinal Chemistry 55, 4489-4500 (2012).

24. Zhang, J. & Peppas, N. A. Molecular interactions in poly (methacrylic acid)/poly (N-isopropyl acrylamide) interpenetrating polymer networks. Journal of Applied Polymer Science 82, 1077-1082 (2001).

25. Mahinroosta, M., Farsangi, Z. J., Allahverdi, A. & Shakoori, Z. Hydrogels as intelligent materials: A brief review of synthesis, properties and applications. Materials Today Chemistry 8, 42-55 (2018).

26. Zhang, Y., Li, Y. and Liu, W. Dipole–dipole and H-bonding interactions significantly enhance the multifaceted mechanical properties of thermoresponsive shape memory hydrogels. Advanced Functional Materials 25, 471-480 (2015).

27. Kim, J., Zhang, G., Shi, M. & Suo, Z. Fracture, fatigue, and friction of polymers in which entanglements greatly outnumber cross-links. Science 374, 212-216 (2021).

28. Wang, Y. et al. A composite hydrogel with high mechanical strength, fluorescence, and degradable behavior for bone tissue engineering. Polymers 11, 1112 (2019).

29. Speight, J. G. Lange's Handbook of Chemistry (McGraw Hill, New York, 2005).

30. Bolan, N. S., Naidu, R., Syers, J. K. & Tillman, R. W. Surface Charge and Solute Interactions in Soils. Advances in Agronomy 67, 87-140 (1999).

31. Tokarev, I. & Minko, S. Stimuli-responsive porous hydrogels at interfaces for molecular filtration, separation, controlled release, and gating in capsules and membranes. Advanced Materials 22, 3446-3462 (2010).

32. Zhao, Z., Wang, C., Yan, H., & Liu, Y. Soft robotics programmed with double crosslinking DNA hydrogels. Advanced Functional Materials 29, 1905911 (2019).

33. Schuch, A. P. & Menck, C. F. M. The genotoxic effects of DNA lesions induced by artificial UV-radiation and sunlight. Journal of Photochemistry and Photobiology B: Biology 99, 111-116 (2010).

34. Hamza, M. A. & Anderson, W. K. Soil compaction in cropping systems: A review of the nature, causes and possible solutions. Soil and Tillage Research 82, 121-145 (2005).

35. Gregory, J. H., Dukes, M. D., Jones, P. H. & Miller, G. L. Effect of urban soil compaction on infiltration rate. Journal of Soil and Water Conservation 61, 117-124 (2006).

Figures

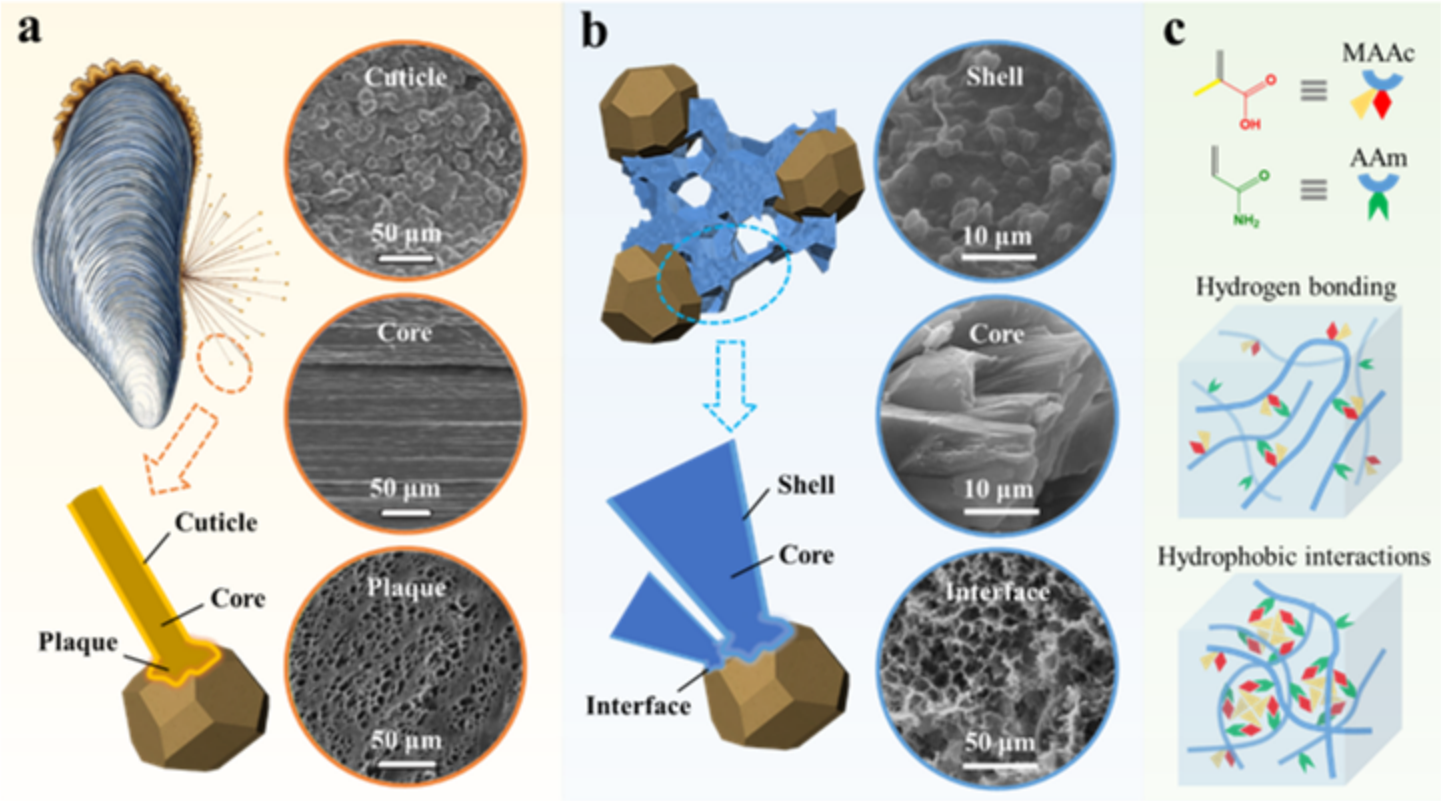

Figure 1

An overview of the mussel mimicry hydrogel. a The scheme of a mussel, a byssal and the SEM image of the cuticle, core and plaque. The SEM images are reproduced with permission from Ref. 19. Copyright CC BY 4.0. **b** The scheme of hydrogel stabilized sand particles and SEM images correspond to the shell, core and interface. Note the scheme is not drawn to scale in order to better illustrate the role of the hydrogel. **c** Scheme of the hydrogen bonding and hydrophobic interactions in the mussel mimicry hydrogel.

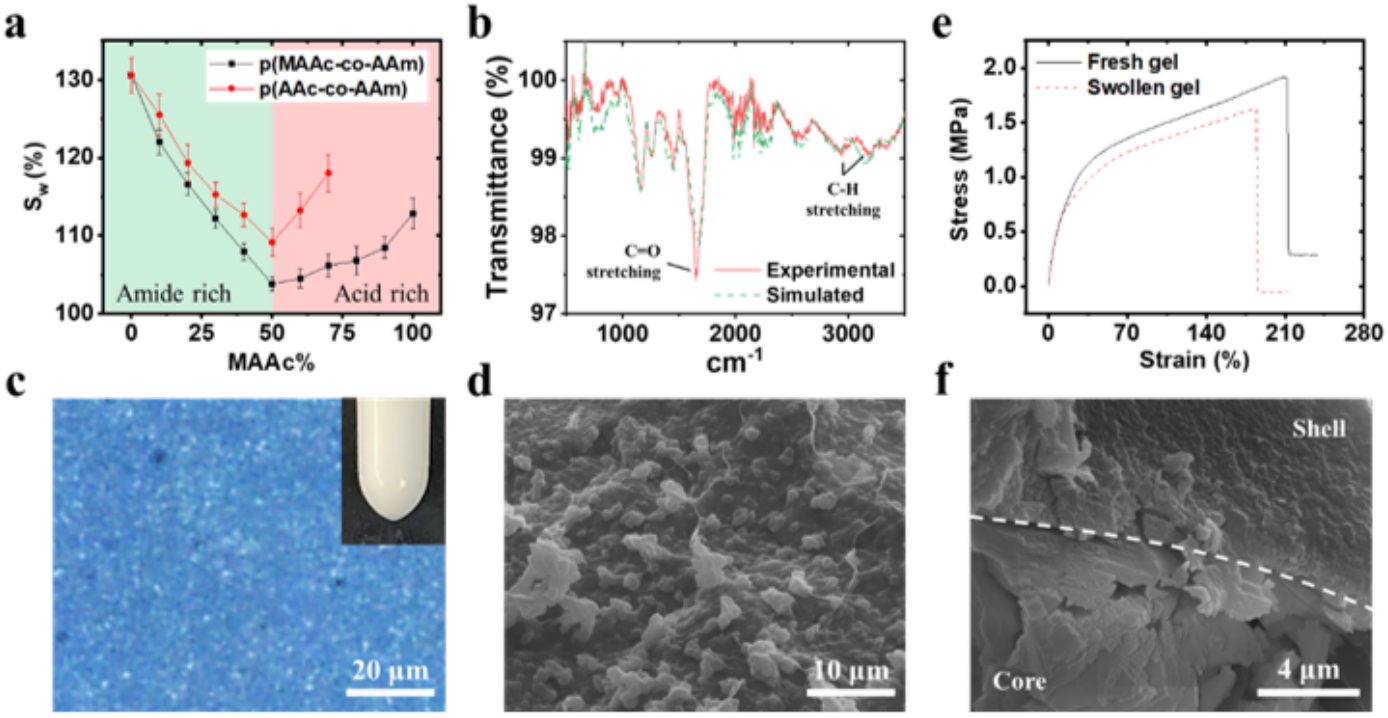

Figure 2

Characteristic properties of the mussel mimicry hydrogel. a The swelling ratio of p(MAAc-co-AAm) and p(AAc-co-AAm) gel of various compositions. **b** The experimental and simulated FT-IR spectra of the mussel mimicry hydrogel. **c** The dark field image of the mussel mimicry hydrogel. Inset: optical image of the cured hydrogel. **d** The SEM image of the shell of the mussel mimicry hydrogel. **e** Tensile tests of freshly prepared and swollen hydrogels. **f** A SEM image showing the core-shell structure of the mussel mimicry hydrogel.

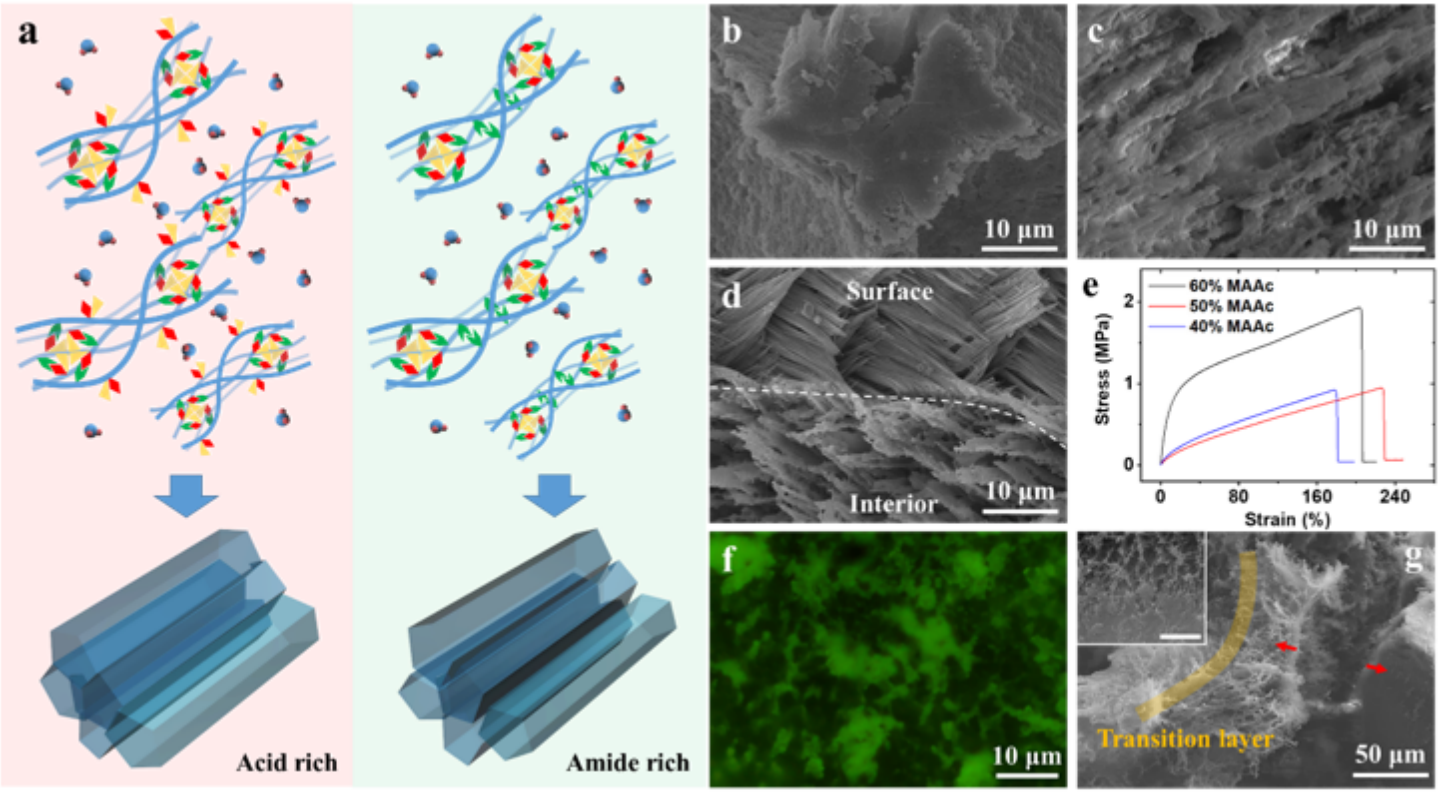

Figure 3

Structural evolution of the synthetic hydrogel. a Scheme of the inter-chain interactions in acid rich and amide rich hydrogel. **b** SEM image of the cross section of an acid rich hydrogel. **c** SEM image of the cross section of an amide rich hydrogel. **d** SEM image of the outer layer of an amide rich hydrogel. **e** Tensile tests of hydrogels with various MAAc contents (E5-E7). **f** Fluorescent microscopic image of a sand particle peeled off from hydrogel stabilized sand columns. **g** SEM image of hydrogel structures in the vicinity of sand particles. The red arrows indicate the detachment between the hydrogel and the sand particle due to external force. Inset: a magnified image showing the structural transition. Scale bar: 5 μm.

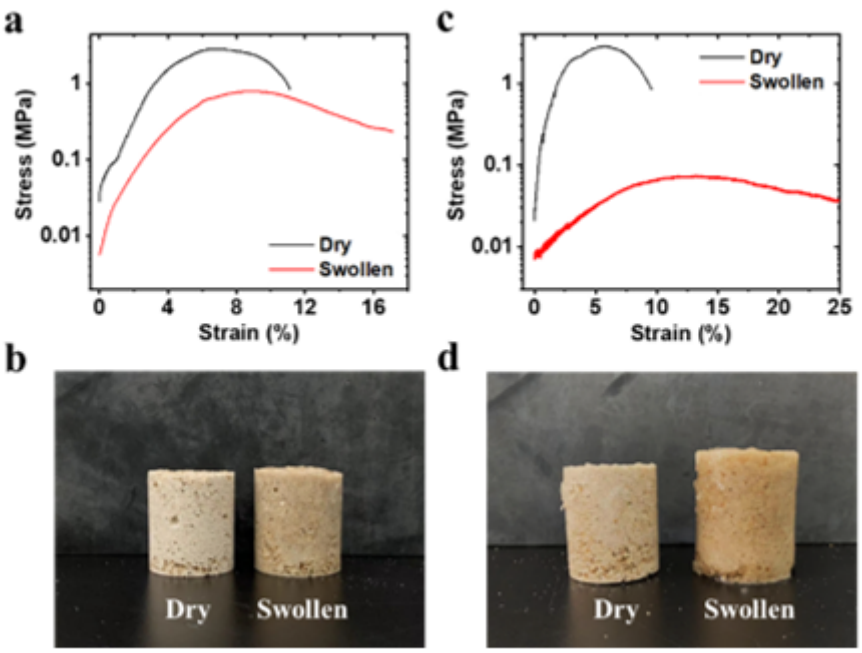

Figure 4

Soil stabilization with hydrogels. **a** The measured UCS of dry and swollen sand columns stabilized with the mussel mimicry hydrogel. **b** A picture of the samples used in a. **c** The measured UCS of dry and swollen sand columns stabilized with conventional hydrogel. **d** A picture of the samples used in c.

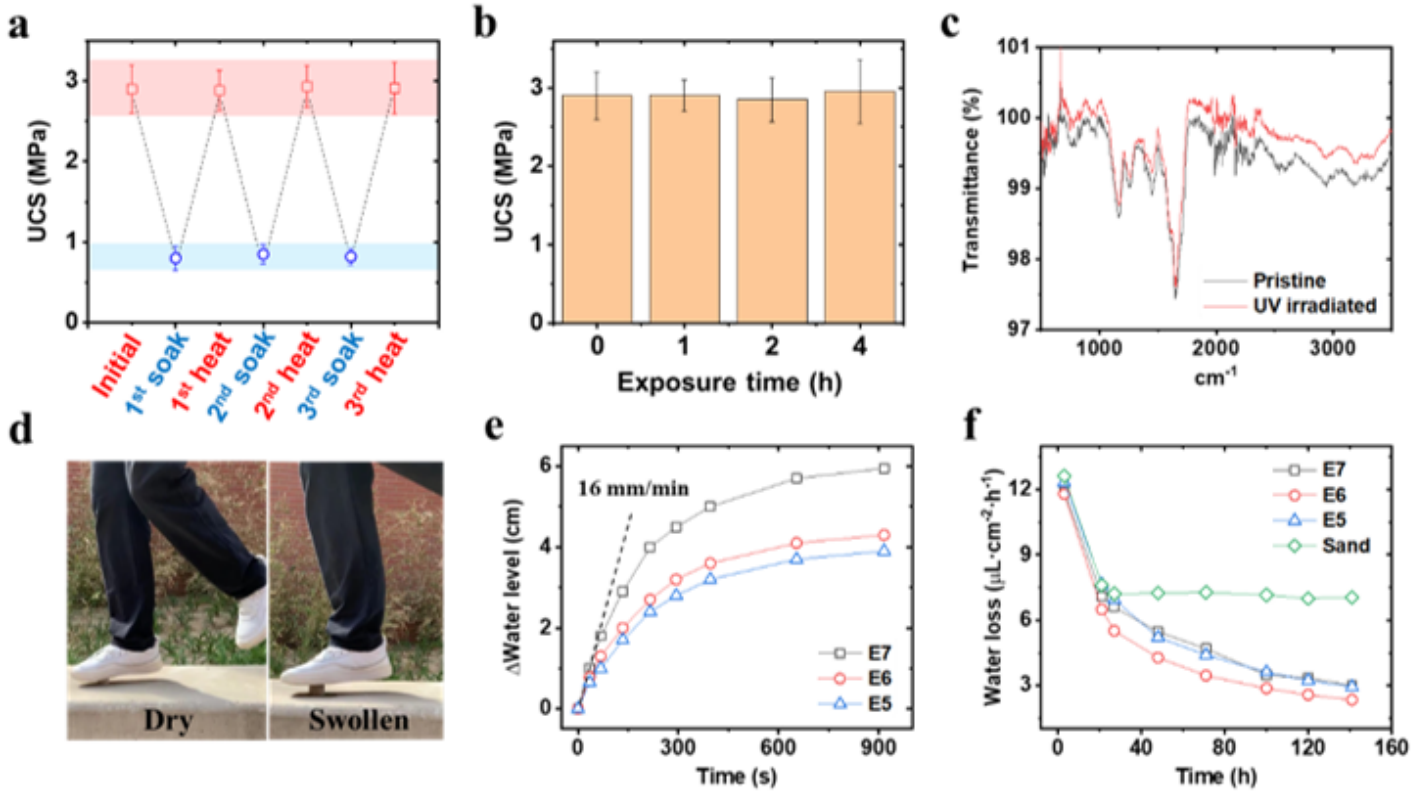

Figure 5

Environmental compatibility tests. **a** UCS of hydrogel stabilized soils under repeated soaking-heating cycles. **b** UCS of hydrogel stabilized soils under intensive UV irradiation. **c** FT-IR spectra of pristine and UV-irradiated hydrogel samples. **d** Pictures showing the robustness of stabilized sand columns after being left outside for a month. **e** Water infiltration performance of sands fixed by precursors E5-E7. **f** Water retention tests for pure sands and sand columns fixed by precursors E5-E7.

Supplementary Files

This is a list of supplementary files associated with this preprint. Click to download.

- Supplementarymaterials.docx